The structure of the metastable $K_{18}Ta_5Zr_5F_{63}$ phase

Miroslav Boča[a, *], Maxim Molokeev[b,d], Aydar Rakhmatullin[c] and Zuzana Netriová[a]

[a] *Institute of Inorganic Chemistry, Slovak Academy of Sciences, Dúbravská cesta 9, SK-845 36 Bratislava, Slovakia*
[b] *Laboratory of Crystal Physics, Kirensky Institute of Physics, Federal Research Center KSC SB RAS, Akademgorodok 50 bld. 38, Krasnoyarsk, 660036, Russia*
[c] *Conditions Extremes et Materiaux: Haute Temperature et Irradiation, 1D avenue de la Recherche Scientifique CS 90055, 45071 Orleans cedex 2, France*
[d] *Siberian Federal University, Krasnoyarsk, 660041, Russia*

[*] *corresponding author: Miroslav Boča, miroslav.boca@savba.sk*

Abstract
A metastable phase $K_{18}Ta_5Zr_5F_{63}$ was prepared by molten salts synthesis of K_2TaF_7 and K_2ZrF_6 in a sealed Pt crucible. The independent part of the unit cell contains two Ta/Zr sites and one pure Zr site. The Ta1/Zr1 ion is coordinated by seven F ions forming one caped trigonal prism. The Ta2/Zr2 ion is coordinated by six F ions forming trigonal prism and this polyhedron is fully ordered. The Zr3 ion is coordinated by six F ions, which are disordered over two positions. All $(Zr/Ta)F_n$ (n=6,7) polyhedra are isolated from each other, however ZrF_6 joint with each other by faces, forming infinity channel along *c*-axis. ^{19}F MAS NMR experiments corresponds with the proposed structural model identifying all five central non-equivalent polyhedron. The $K_{18}Ta_5Zr_5F_{63}$ phase decomposes within several months to its initial components that can be monitored by NMR, DSC and XRD experiments. Moreover, accelerated decomposition can be achieved by thermal treatment, however under the formation of K_3ZrF_7 phase.

Keywords
Molten salts synthesis, K_2ZrF_6, K_2TaF_7, phase transition, single crystal analysis, XRD, DSC, ^{19}F MAS NMR

Introduction
Chemistry of ternary fluorides is a very wide and complex topic including hundreds of compounds (all d- and f- elements and some part of p-elements) and tens of investigation methods. Many reviews were published *e.g.* [1-4]. Some of these compounds can be characterized by strong tendency to form island like polyhedrons where all fluorine atoms are terminally bonded. Such a group can be represented by tantalum or niobium fluorides *e.g.* [5]. We are not aware of any compound of this family containing bridging fluorine atoms. The situation changes when also oxygen atoms are present besides fluorine atoms *e.g.* in $K_2Ta_4O_9F_4$ or $K_6Ta_{6.5}O_{14}F_{9.5}$ [6, 7] compounds, where either only oxygen or both oxygen and fluorine atoms can serve as bridging elements. However, the structures with island like polyhedron still dominate. Contrary, there is a group of compounds with high tendency to form infinite structural motives of the D1, D2 or even D3 dimension. Such a group can be represented by zirconium fluorides described *e.g.* in [8] and refs. therein.

The aim of this work was to try to force the bridging behaviour to the rigid central atom of tantalum using zirconium as co-partner *i.e.* the central atom preferring the bridging mode. Thus the compounds K_2TaF_7 and K_2ZrF_6 were selected as suitable candidates.

Experimental

Preparation of sample: For the preparation of the sample, the following chemicals were used:

K_2TaF_7 was prepared at the Institute of Chemistry and Technology of Rare Elements and Minerals, RAS Apatite-Russia, 99.5 %). K_2ZrF_6 was prepared according to [9].

The finely powdered and homogenized mixture of K_2TaF_7 (0.830 g, 2.15 mmol) and K_2ZrF_6 (0.609 g, 2.15 mmol) was placed in a specially arranged platinum crucible with a sealed lid. The narrow platinum tube on the top of the lid, which served for loading of the sample into the crucible, was closed first by clamping and then by welding. Homogenizing and weighing the sample was done in a glove box under dry inert atmosphere. The crucible was placed in a furnace and heated to 1153 K at a rate of 5 K min^{-1} and then heated to 1173 K at a rate of 1 K min^{-1}. The temperature of the furnace was kept at 1173 K for 120 min and cooled at a rate of 1 K min^{-1} to room temperature. Platinum crucible was opened and the sample was separated as white cake. Several single crystals were separated by sieving and the rest was powder for other diffraction and spectroscopic investigation.

Structural analysis: The intensity patterns were collected from single crystals $K_{18}Ta_5Zr_5F_{63}$ at 296 K using the SMART APEX II X-ray single crystal diffractometer (Bruker AXS, analytical equipment of Krasnoyarsk Center of collective use of SB RAS) equipped with a CCD-detector Photon2, graphite monochromator and Mo Kα radiation source. The absorption corrections were applied using the SADABS program. The structures were solved by the direct methods using package SHELXS and refined in the anisotropic approach for heavy atoms and isotropic approach for F ions using the SHELXL program [10]. The structure test for the presence of missing symmetry elements and possible voids was produced using the program PLATON [11]. The DIAMOND program is used for the crystal structure plotting [12].

Powder X-ray diffraction: XRD data of $K_{18}Ta_5Zr_5F_{63}$ were obtained using diffractometer D8 ADVANCE (Bruker, analytical equipment of Krasnoyarsk Center of collective use of SB RAS) equipped by a VANTEC detector with a Ni filter and Cu Kα radiation source. An attachment Anton Paar TTK450 was used for all temperature measurements in the range of 153-633 K (Figure 1a, b). Each pattern was measured in the 2θ range of 5-90º with 0.6mm divergence slit, the step size of 2θ was 0.016°, and the counting time was 0.4 s per step. The Le Bail profile fitting was produced using program TOPAS 4.2 [13]. Low *R*-factors and good refinement results shown in (Table 1S, Figure 1c) indicate the crystal structures of the powder samples to be representative one of the $K_{18}Ta_5Zr_5F_{63}$ bulk structure.

DSC analysis: The thermal properties of the studied compounds were investigated by means of the DSC methods performed with a NETZSCH Simultaneous Thermal Analyzer STA 449 F1 Jupiter®. The sample (m_0 ≈ 20.45 mg) was placed in a Pt/Rh (80/20) crucible and enclosed in an STA apparatus. The system was three times evacuated and then measured under argon atmosphere (244 mL·min^{-1}). The experimental thermogram was recorded at temperature regime ranging from 293 K to 1173 K and back with heating/cooling rate of 5 K·min^{-1}. A baseline correction measurement for the empty crucible was done under the same conditions as the sample measurements. Calibration of temperature (for Pt crucibles) and sensitivity (± 3%) was done for the compounds $C_{12}H_{10}$, $RbNO_3$, Ag_2SO_4, CsCl, K_2CrO_4 and $BaCO_3$. The NETZSCH Proteus Thermal Analysis software was used for data processing and for evaluation of the experimental thermogram.

X-ray Photoelectron Spectroscopy: XPS signals were recorded using a Thermo Scientific K-Alpha XPS system (Thermo Fisher Scientific, UK) equipped with a micro-focused, monochromatic Al Kα X-ray source (1486.6 eV). An X-ray beam of 100 μm size was used at 1.16 mA x 12 kV. The spectra were acquired in the constant analyzer energy mode with pass energy of 50 eV for the whole region ranging from -10 eV to

1100 eV with the energy step size of 0.1 eV. Charge compensation was achieved with a flood gun incorporated into the system, which provides low energy electrons (~0 eV) and low energy argon ions (20 eV) from a single source. The argon partial pressure was 2 x 10^{-7} mbar in the analysis chamber. Position of C 1s signal of adventitious carbon was for all samples 284.7 eV, so it was not necessary to do charge correction using this internal reference. The Thermo Scientific *Avantage* software, version 5.948 (Thermo Fisher Scientific), was used for digital acquisition and data processing. Spectral calibration was carried out by using the automated calibration routine and the internal Au, Ag and Cu standards supplied with the K-Alpha system. The Powel fitting algorithm was used with 100 iterations to fit the XPS F1s peaks. The line shapes were products of a Lorentz/Gauss mixture, with the ratio fixed at L/G = 45%. This value was taken from fitting the F1s peak of pure NaF, with this parameter permitted to vary using the Powel algorithm.

NMR spectroscopy: Room temperature ^{19}F NMR spectra were recorded on a Bruker AVANCE Neo 850 NMR spectrometer with a 20 T magnet operating at 800.0 MHz for ^{19}F nuclei. Standard Bruker MAS probehead was used with 1.3-mm rotor, where powder was rotated at 60 kHz. ^{19}F chemical shift was referenced to a $CFCl_3$.

Results

Crystal structures of $K_{18}Ta_5Zr_5F_{63}$

The unit cell of $K_{18}Ta_5Zr_5F_{63}$ corresponds to trigonal/hexagonal symmetry. Initially space group *P*-3 was determined from the statistical analysis of the reflection intensities. Crystal structure was solved, but refinement was not good. The Bragg R_B-factor didn't decrease lower than 16 %. The twinning of single crystal with rotation of unit cell around [210] direction in real space (Figure 1S) was detected by PLATON program. Further refinement using the twin matrix rotation (0 1 0; 1 0 0; 0 0 -1) dropped R_B-factor up to 9 %. The ratio of twinned blocks was 54:46. After that the structure test for the presence of missing symmetry elements in PLATON revealed several additional elements and the structure was transformed to $P6_3/m$ space group. It should be noted that trying to solve crystal structure in $P6_3/m$ space group failed due to twinning. Anyway our nontrivial route led to correct structure and stable refinement. The main crystal data are shown in Table 1. The atom coordinates and main bond lengths are shown in Table 2S and Table 3S, respectively.

The independent part of the unit cell contains two Ta/Zr sites: Ta1/Zr1 (6*h* Wyckoff site with *m* local symmetry) and Ta2/Zr2 (2*c* site with -6 symmetry) (Figure 2) in which the Ta/Zr ratio was refined up to 0.69(2):0.31(2) and 0.52(2):0.48(2), respectively. In addition there is one pure Zr site (2*a* site with -6 local symmetry). Thus the Ta:Zr ratio in compound appeared to be 5.18:4.82. There are three K sites in the structure, all in 6*h* Wyckoff site with *m* local symmetry. There are seven F ions in the asymmetric part of the unit cell, and two sites (F5 and F7) are occupied by half. The total amount of F ions in the unit cell is 63 and the chemical formulae can we written as $K_{18}Ta_{5.18}Zr_{4.82}F_{63}$ or simplified to $K_{18}Ta_5Zr_5F_{63}$. The sum of charge is zero: 18+5*(4+5)-63 = 0 and this additionally proves correctness of the structure. The Ta1/Zr1 ion is coordinated by seven F ions forming one caped trigonal prism. It should be noted that F5 ion forms cap of this prism, and this site is occupied by half only. One can suggest that one unit cell can contain $(Ta1/Zr1)F_6$ prism and another unit cell can contain $(Ta1/Zr1)F_7$ one caped prism in the crystal. The X-ray averages structure over the space and time leading to $(Ta1/Zr1)F_6F_{0.5}$ polyhedron. The Ta2/Zr2 ion is coordinated by six F ions forming trigonal prism and this polyhedron is fully ordered. The Zr3 ion is coordinated by twelve F ions, which originated from one F7 ion by multiplication symmetry elements. Since F7 has occupancy 0.5, therefore, really, the Zr3 ion is coordinated by six F ions, which are disordered over two positions. Taking into account all these facts we can suggest that structure is disordered. All $(Zr/Ta)F_n$ (n=6,7) polyhedra are isolated from each other,

however ZrF_6 joint with each other by faces, forming infinity channel along *c*-axis (Figure 2).

It should be noted that if equimolar amounts of both compounds would be considered the resulting formula should be K_4TaZrF_{13} or $K_{20}Ta_5Zr_5F_{65}$. It means that during the experiment more stable system was formed, however poorer of two KF "molecules" what represents 3 wt % difference with $K_{18}Ta_5Zr_5F_{63}$. Such a situation might be compare to the system NaF-ZrF_4 in which equimolar amounts of NaF and ZrF_4 does not give rise to $NaZrF_5$ but rather to more stable $Na_7Zr_6F_{31}$ phase [14].

XPS spectroscopy provided the ratio of elements as follow: Ta/Zr is 1/1 *vs.* 1.07(exp.); F/K is 63/18 vs. 3.00(exp.); K/Ta is 18/5 *vs.* 5.65(exp.); F/Ta is 63/5 *vs.* 17.00(exp.) what is in acceptable agreement between structural formula and theoretical ratio (giving into the consideration difference for light and heavy elements, the powdered nature of the sample). Moreover, also presence of both terminal and bridging form of fluorine atoms were identified in line with the structural investigation and in context of the methodology of sensitivity to various bonding modes of fluorine atom [14].

NMR spectroscopy. The room temperature polymorph contains seven fluorine sites. ^{19}F MAS NMR spectra revealed two groups of resonances. Appling very fast spinning frequency (60 kHz) and high field (20.0 T) has enabled us to obtain only five signals with a Gaussian line shape. By considering the Ta and Zr atoms surroundings, it can be seen that the five Ta and Zr atomic positions have one or few distinct fluorine atoms in their coordination spheres: Ta1(2F1, 2F2, 2F3, F4, 0.5F5), Zr1(2F1, 2F2, 2F3, F4, 0.5F5), $Ta2(F6)_6$, $Zr2(F6)_6$, $Zr3(0.5F7)_{12}$. Considering fast hoping of the fluorine on each position around one polyhedron, the ^{19}F δ_{iso} is then the barycenter of the individual δ_{iso}. Thus, five peaks we assigned to fluorine atoms in five polyhedra. Low field signals have the chemical shift values close to K_2TaF_7 (17.1 ppm) and K_3TaF_8 (17.3 ppm) compounds [5] and we attribute them to fluorine atoms connected with Ta atoms. High field peaks can be assigned to fluorine atoms connected with Zr atoms (ref). The intensity ratio of the two environments I[Ta]/I[Zr] = 0.53/0.47 is in rather good agreement with the value of 0.518/0.482 expected from the sites multiplicities and the sites occupations. There are differences between expected and observed integral data for the tantalum polyhedra. A possible reason for this ambiguity is a signal-overlay. The reasonably good agreement between the expected and experimental integral intensities enables to perform spectral assignment of the NMR resonances with the crystallographic sites. Small amounts of a secondary unknown phase were observed at 13.4 ppm.

Note: During high temperature MAS NMR experiments both BN and AlN crucibles were damaged by the sample thus high temperature experiments could not be performed.

Table N. Experimental ^{19}F MAS NMR isotropic chemical shifts δ_{iso}, Integral intensities, and calculated integral intensities.

	δ_{iso}, ppm (±0.1 ppm)	Integral intensity, % (± 1%)	Calculated Integral intensity, %
Ta2	15.9	19	10.4
Ta1	15.1	34	41.4
Zr1	-16.7	17	18.6
Zr3	-17.6	18	20.0
Zr2	-18.8	12	9.6

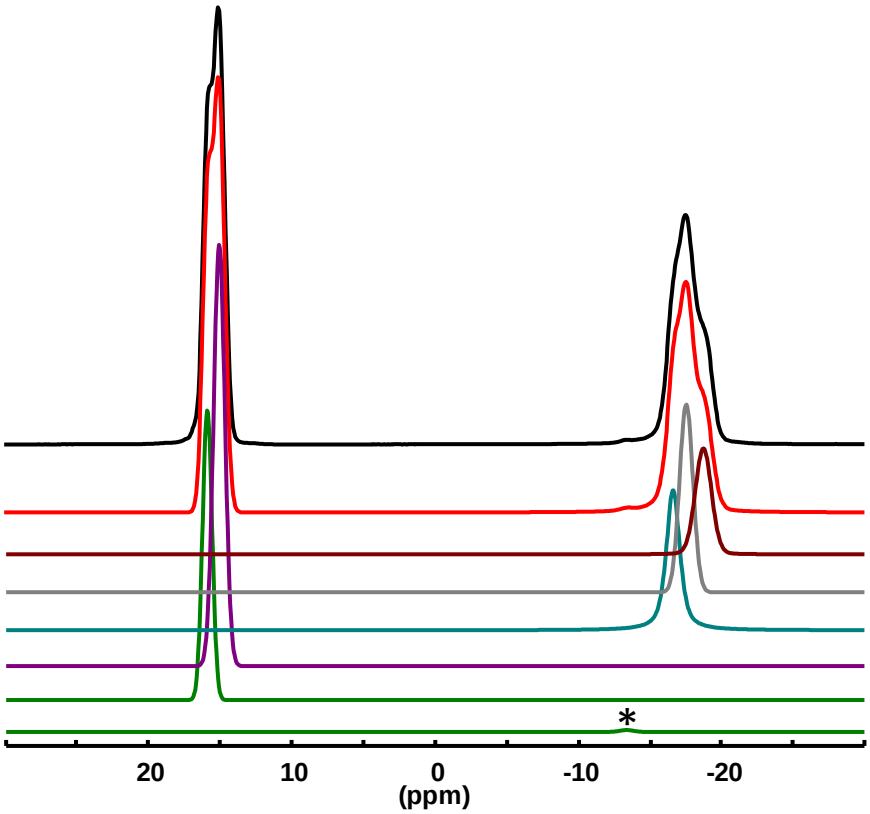

Figure XN. ^{19}F MAS NMR experimental (black line) spectrum and its simulation (colour lines). (* secondary phase).

It must be noted that the sample undergo to thermal decomposition as well as to time decomposition. XRD of the sample measured three months after the synthesis shoved almost complete decomposition to the initial phases K_2TaF_7 and K_2ZrF_6. This process supports the idea made from NMR about the fast hoping of the fluorine on various position resulting to the stabilisation of the system.

DSC measurements. DSC measurements on fresh sample showed the presence of one weak endothermic effect at 801 K (0.1505 J/g equal to 493.3 J/mol) on heating regime up to 827 K. This target temperature was selected from the phase diagram of K_2TaF_7-K_2ZrF_6 far below the liquid phase of the $x(K_2TaF_7)$ = 0.5 point [15]. However, during the cooling regime no identifiable effect was observed. XRD of the sample treated by DSC experiment showed the presence of $K_{18}Ta_5Zr_5F_{63}$ together with some small amount of K_3ZrF_7.

DSC treatment of the one months old sample heated up to 1173 K showed three endothermic effects at 940 K, 961 K and 988 K (this last one can be attributed to melting). The existence of such three effects was documented for pure K_2TaF_7 phase (however with somewhat higher temperatures) [16-18]. XRD of the solidified sample showed the presence of $K_{18}Ta_5Zr_5F_{63}$ together with K_3ZrF_7 as majority phase in this case.

DSC treatment of two months old sample revealed two endothermic signals at 507 K and 555 K that are quite similar to pure K_2ZrF_6 [9]. At ca 1023 K the sample starts to evaporate with the mass loss of ca 25 wt % up to 1173 K. Some other three not well resolved and overlapping endothermic effects at 884 K, 935 K, and 958 K were observed, as well typical for K_2TaF_7 phase but even at lower temperatures as in the case of one month old sample.

The X-ray powder pattern transformation under sample heating is presented in the Figure 1. One can see that additional peaks appeared at 543 K (Figure 1b). Their

intensities increase under further heating. The main phase $K_{18}Ta_5Zr_5F_{63}$ peaks totally disappear at 663 K and the rest peaks were associated with the cubic phase *Fm*-3*m* isostructural to K_3ZrF_7. Thermal dependencies of main phase cell parameters *a*, *c* (Figure 3) show linear tread only in the range of 303-543 K. Therefore, the $K_{18}Ta_5Zr_5F_{63}$ phase is stable up to 543 K only and further heating decomposes it, leading to cubic phase formation, which is isostructural to K_3ZrF_7.

Conclusions

Metastable phase $K_{18}Ta_5Zr_5F_{63}$ was prepared by molten salts synthesis from K_2TaF_7 and K_2ZrF_6. Its structure was solved based on single crystal structural analysis and suggested model was confirmed by ^{19}F MAS NMR experiments. Time dependent decomposition of the metastable phase was observed when under isothermal conditions at ambient temperature the phase decompose to its initial phases while during thermal treatment and decomposition K_3ZrF_7 phase is formed as one of the product.

Supplementary data

The crystallographic data for the structural analysis have been deposited with Cambridge Crystallographic Data Centre CSD # 1964932. The information may be obtained free of charge from The Director, CCDC, 12 Union Road, Cambridge CB2 1EZ, UK (Fax: +44(1223)336-033, E-mail: deposit@ccdc.cam.ac.uk, or www: www.ccdc.cam.ac.uk).

Acknowledgments

Financial support from the TGIR-RMN-THC Fr3050 CNRS for conducting the research is gratefully acknowledged. This work was supported by the Slovak Research and Development Agency under the contract No. APVV-15-0479. This work was financially supported by the Scientific Grant Agency of the Ministry of Education of the Slovak Republic and the Slovak Academy of Sciences, No Vega 2/0114/16.

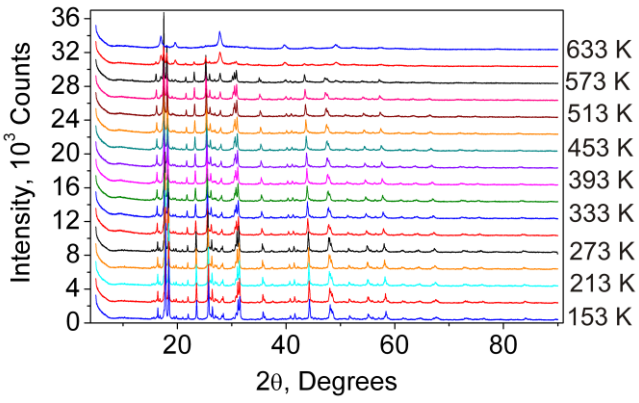

a)

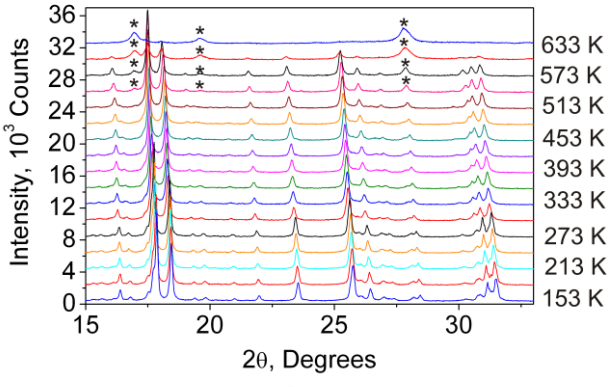

b)

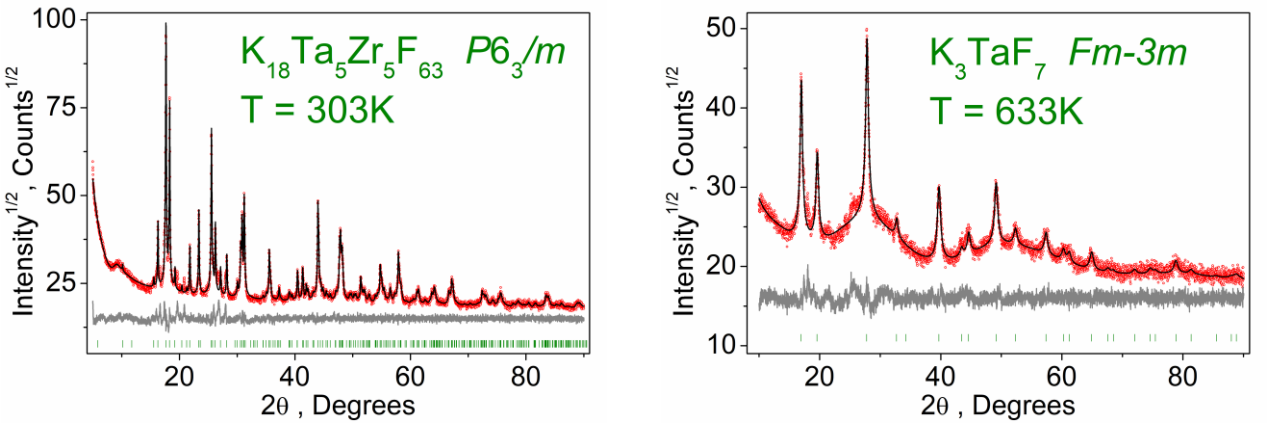

Figure 1. The X-ray pattern transformation of $K_{18}Ta_5Zr_5F_{63}$ under heating from 153 K to 633 K (a). Zoomed part of these patterns (b) revealed appearance of impurity peaks (marked by stars) at 543 K, which can be associated with K_3ZrF_7 isostructural phase. The main peak intensities of $K_{18}Ta_5Zr_5F_{63}$ decrease from 543 to 633 K and totally disappear at 633 K. Thus $K_{18}Ta_5Zr_5F_{63}$ transforms to the cubic phase isostructural to K_3ZrF_7. Difference Rietveld plots of $K_{18}Ta_5Zr_5F_{63}$ at 303 K (c) and K_3ZrF_7 at 633 K (d) showed that these two end phases are almost pure.

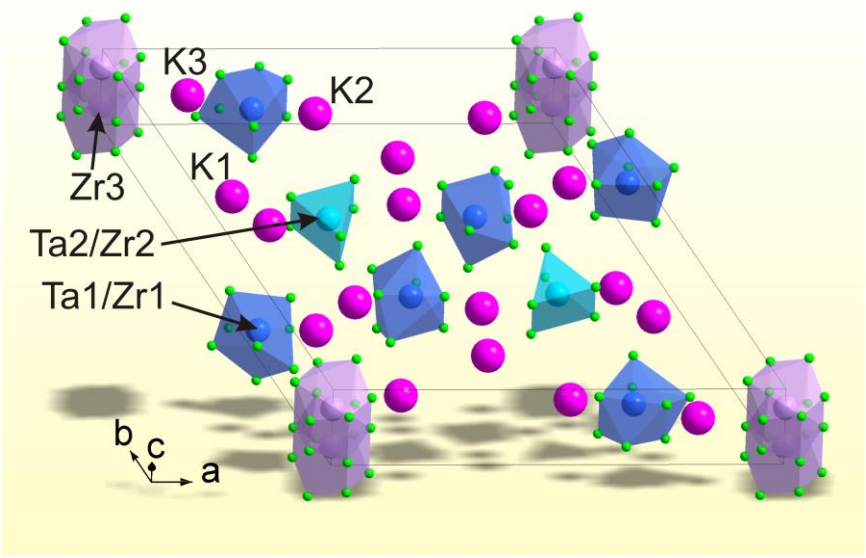

Figure 2. The crystal structure of the $K_{18}Ta_5Zr_5F_{63}$. The heavy ions in the asymmetric unit are labelled.

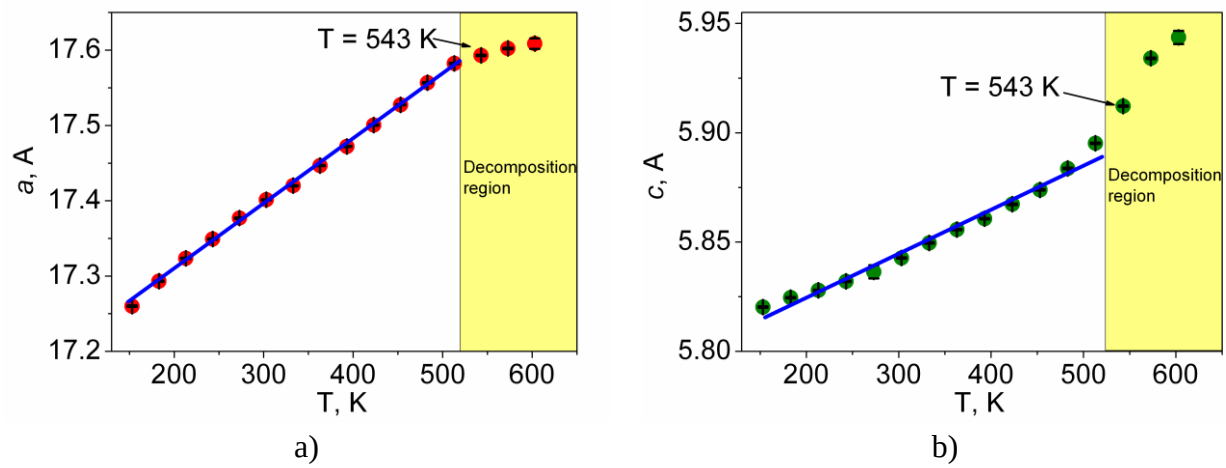

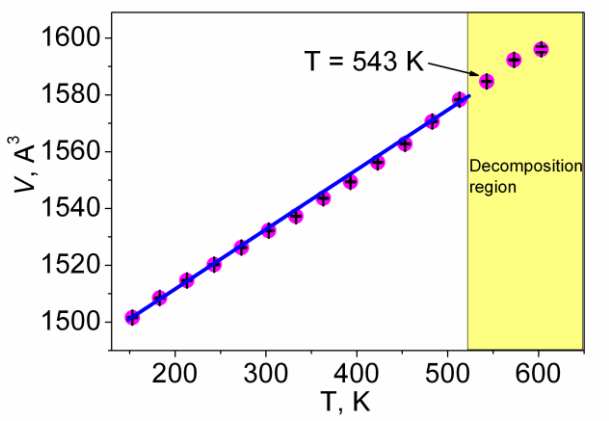

c)

Figure 3. Thermal dependencies of cell parameters per T: (a) *a* cell parameter; (b) *c* cell parameter; (c) cell volume *V*(T).

Table 1. Crystal structure parameters of $K_{18}Ta_5Zr_5F_{63}$

Sum formula	$F_{63}K_{18}Ta_{5.18}Zr_{4.82}$
Dimension (mm)	0.25×0.2×0.1
Color	Colorless
Molecular weight	3277.80
Temperature (K)	296
Space group, *Z*	$P6_3/m$, 1
a (Å)	17.3782 (8)
c (Å)	5.8377 (3)
V (Å^3)	1526.80 (16)
ρ_{calc} (g/cm^3)	3.565
μ (mm^{-1})	11.458
Reflections measured	22649
Reflections independent	1702
Reflections with $F > 4\sigma(F)$	1647
$2\theta_{max}$ (°)	61.072
h, *k*, *l* - limits	-24 ≤ *h* ≤ 24; -24 ≤ *k* ≤ 24; -8 ≤ *l* ≤ 8
R_{int}	0.0583
The weighed refinement of F^2	$w=1/[\sigma^2(F_o^2)+(0.076P)^2+58.01P]$, where $P=(F_o^2+2F_c^2)/3$
Number of refinement parameters	60
$R1$ [$F_o > 4\sigma(F_o)$]	0.0855
*wR*2	0.2241
Goof	1.223
$\Delta\rho_{max}$ (e/Å^3)	2.423
$\Delta\rho_{min}$ (e/Å^3)	-2.832
Extinction coefficient	0.0009 (3)
$(\Delta/\sigma)_{max}$	<0.001

Supported Information

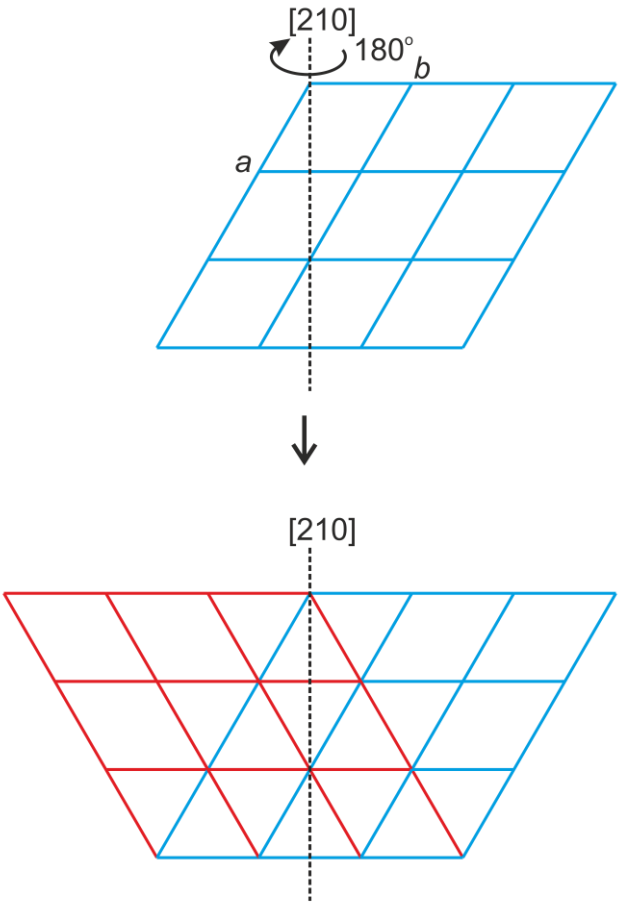

Figure 1S. The twining mechanism in $K_{18}Ta_5Zr_5F_{63}$. The unit cell rotates around [210] direction in real space. The ratio of twinned block is close to 0.5:0.5.

Table 1S. Main parameters of processing and refinement of the $K_{18}Ta_5Zr_5F_{63}$ and K_3ZrF_7

T, K	Phase	Space group	Cell parameters (º, Å), Cell volume (Å^3)	R_{wp}, R_p (%), χ^2
153	$K_{18}Ta_5Zr_5F_{63}$	$P6_3/m$	a = 17.2600 (9), c = 5.8203 (3), V = 1501.6 (2)	9.51, 6.65, 2.43
183	$K_{18}Ta_5Zr_5F_{63}$	$P6_3/m$	a = 17.2933 (8), c = 5.8246 (3), V = 1508.5 (2)	9.25, 6.53, 2.37
213	$K_{18}Ta_5Zr_5F_{63}$	$P6_3/m$	a = 17.3236 (8), c = 5.8279 (3), V = 1514.7 (2)	8.86, 6.21, 2.27
243	$K_{18}Ta_5Zr_5F_{63}$	$P6_3/m$	a = 17.3491 (8), c = 5.8320 (3), V = 1520.2 (2)	8.65, 6.10, 2.21
273	$K_{18}Ta_5Zr_5F_{63}$	$P6_3/m$	a = 17.3770 (9), c = 5.8364 (3), V = 1526.2 (2)	8.60, 6.02, 2.19
303	$K_{18}Ta_5Zr_5F_{63}$	$P6_3/m$	a = 17.4023(9), c = 5.8430(3),	6.24, 4.57, 1.61

333	$K_{18}Ta_5Zr_5F_{63}$	*P*6$_3$/*m*	*V* = 1532.4(2) *a* = 17.4201(7), *c* = 5.8496(3), *V* = 1537.29(15)	6.20, 4.51, 1.60
363	$K_{18}Ta_5Zr_5F_{63}$	*P*6$_3$/*m*	*a* = 17.4468(8), *c* = 5.8557(3), *V* = 1543.62(16)	6.10, 4.47, 1.58
393	$K_{18}Ta_5Zr_5F_{63}$	*P*6$_3$/*m*	*a* = 17.4721(7), *c* = 5.8607(3), *V* = 1549.41(15)	5.95, 4.38, 1.53
423	$K_{18}Ta_5Zr_5F_{63}$	*P*6$_3$/*m*	*a* = 17.5006(8), *c* = 5.8673(3), *V* = 1556.23(15)	5.87, 4.33, 1.51
453	$K_{18}Ta_5Zr_5F_{63}$	*P*6$_3$/*m*	*a* = 17.5274(7), *c* = 5.8739(3), *V* = 1562.75(15)	6.34, 4.76, 1.62
483	$K_{18}Ta_5Zr_5F_{63}$	*P*6$_3$/*m*	*a* = 17.5567(8), *c* = 5.8837(3), *V* = 1570.62(17)	5.82, 4.30, 1.49
513	$K_{18}Ta_5Zr_5F_{63}$	*P*6$_3$/*m*	*a* = 17.5824(8), *c* = 5.8952(3), *V* = 1578.29(16)	5.54, 4.19, 1.42
543	$K_{18}Ta_5Zr_5F_{63}$	*P*6$_3$/*m*	*a* = 17.5930(7), *c* = 5.9122(2), *V* = 1584.74(15)	5.05, 3.92, 1.29
	K_3ZrF_7	*Fm*-3*m*	*a* = 9.07(2), *V* = 746(5)	
573	$K_{18}Ta_5Zr_5F_{63}$	*P*6$_3$/*m*	*a* = 17.6022(8), *c* = 5.9340(3), *V* = 1592.26(18)	5.11, 4.03, 1.31
	K_3ZrF_7	*Fm*-3*m*	*a* = 9.073(3), *V* = 746.9(7)	
603	$K_{18}Ta_5Zr_5F_{63}$	*P*6$_3$/*m*	*a* = 17.609(7), *c* = 5.944(3), *V* = 1596(1)	4.70, 3.68, 1.19
	K_3ZrF_7	*Fm*-3*m*	*a* = 9.069(4), *V* = 746(1)	
633	K_3ZrF_7	*Fm*-3*m*	*a* = 9.0778(3), *V* = 748.1(6)	5.53, 4.34, 1.28

Table 2S. Fractional atomic coordinates and isotropic or equivalent isotropic displacement parameters (Å^2) of $K_{18}Ta_5Zr_5F_{63}$

Atom	*x*	*y*	*z*	U_{iso}*/U_{eq}	Occ.
Ta1	0.34021(9)	0.32871(11)	3/4	0.0277(4)	0.69(2)
Zr1	0.34021(9)	0.32871(11)	3/4	0.0277(4)	0.31(2)
Ta2	2/3	1/3	3/4	0.0289(7)	0.52(2)
Zr2	2/3	1/3	3/4	0.0289(7)	0.48(2)
Zr3	0	0	1/4	0.0440(16)	1
K1	0.2674(4)	0.4220(4)	1/4	0.0369(13)	1
K2	0.5379(5)	0.4026(5)	1/4	0.0482(17)	1
K3	0.2295(10)	0.1487(8)	1/4	0.104(5)	1
F1	0.2440(9)	0.2843(9)	0.524 (3)	0.061(4)*	1

F2	0.402(2)	0.4231(19)	0.504 (7)	0.132(9)*	1
F3	0.3903(13)	0.2822(12)	0.543 (4)	0.099(6)*	1
F4	0.296(2)	0.409(3)	3/4	0.124(12)*	1
F5	0.227(4)	0.194(4)	3/4	0.081(14)*	0.5
F6	0.5727(16)	0.2609(16)	0.554 (5)	0.127(8)*	1
F7	0.091(3)	0.079(3)	0.051 (8)	0.092(12)*	0.5

Table 3S. Main geometric parameters (Å) of $K_{18}Ta_5Zr_5F_{63}$

Ta1—F3	1.89(2)	K1—F4	2.988(8)
Ta1—F3^{i}	1.89(2)	K1—F4^{xxiii}	2.988(8)
Ta1—F1	1.958(15)	K1—F6^{xxi}	2.60(3)
Ta1—F1^{i}	1.958(15)	K1—F6^{xxii}	2.60(3)
Ta1—F4	1.90(4)	K1—F1^{xi}	2.736(16)
Ta1—F5	2.18(6)	K1—F1	2.736(16)
Ta1—F2^{i}	2.04(4)	K1—F3^{xxii}	2.81(2)
Ta1—F2	2.04(4)	K1—F3^{xxi}	2.81(2)
Ta2—F6^{v}	1.87(3)	K1—F2	2.77(3)
Ta2—F6^{vi}	1.87(3)	K1—F2^{xi}	2.77(3)
Ta2—F6^{i}	1.87(3)	K1—Zr2^{x}	3.811(6)
Ta2—F6	1.87(3)	K1—Ta2^{x}	3.811(6)
Ta2—F6^{vii}	1.87(3)	K2—F2^{xi}	2.95(3)
Ta2—F6^{viii}	1.87(3)	K2—F2	2.95(3)
Zr3—F7^{xi}	1.89(4)	K2—F3^{xi}	2.92(2)
Zr3—F7^{xii}	1.89(4)	K2—F3	2.92(2)
Zr3—F7^{xiii}	1.89(4)	K2—F2^{x}	3.03(3)
Zr3—F7^{xiv}	1.89(4)	K2—F2^{xxiv}	3.03(3)
Zr3—F7^{xv}	1.89(4)	K2—F6^{viii}	3.01(3)
Zr3—F7	1.89(4)	K2—F6^{xxv}	3.01(3)
Zr3—F7^{xvi}	2.30(4)	K2—F4^{x}	3.10(4)
Zr3—F7^{iv}	2.30(4)	K2—F6	3.33(3)
Zr3—F7^{xvii}	2.30(4)	K2—F6^{xi}	3.33(3)
Zr3—F7^{xviii}	2.30(4)	K2—Ta1^{x}	4.050(7)
Zr3—F7^{xix}	2.30(4)	K3—F7	2.38(4)
Zr3—F7^{xx}	2.30(4)	K3—F7^{xi}	2.38(4)
		K3—F1	2.754(16)
		K3—F1^{xi}	2.754(16)
		K3—F1^{xxvi}	2.826(16)
		K3—F1^{iii}	2.826(16)
		K3—F5^{iii}	2.89(6)
		K3—F5^{xxiii}	3.030(15)
		K3—F5	3.030(15)
		K3—F3^{xi}	3.10(2)
		K3—F3	3.10(2)
		K3—F7^{xviii}	3.23(5)

Symmetry codes: (i) *x*, *y*, -*z*+3/2; (ii) *x*, *y*, *z*+1; (iii) *y*, -*x*+*y*, -*z*+1; (iv) *x*-*y*, *x*, *z*+1/2; (v) -*y*+1, *x*-*y*, -*z*+3/2; (vi) -*y*+1, *x*-*y*, *z*; (vii) -*x*+*y*+1, -*x*+1, -*z*+3/2; (viii) -*x*+*y*+1, -*x*+1, *z*; (ix) *x*-*y*+1, *x*, *z*+1/2; (x) -*x*+1, -*y*+1, -*z*+1; (xi) *x*, *y*, -*z*+1/2; (xii) -*x*+*y*, -*x*, *z*; (xiii) -*y*, *x*-*y*, *z*; (xiv) -*y*, *x*-*y*, -*z*+1/2; (xv) -*x*+*y*, -*x*, -*z*+1/2; (xvi) -*x*, -*y*, -*z*; (xvii) *y*, -*x*+*y*, *z*+1/2; (xviii) *y*, -*x*+*y*, -*z*; (xix) *x*-*y*, *x*, -*z*; (xx) -*x*, -*y*, *z*+1/2; (xxi) *x*-*y*, *x*, -*z*+1; (xxii) *x*-*y*, *x*, *z*-1/2; (xxiii) *x*, *y*, *z*-1; (xxiv) -*x*+1, -*y*+1, *z*-1/2; (xxv) -*x*+*y*+1, -*x*+1, -*z*+1/2; (xxvi) *y*, -*x*+*y*, *z*-1/2.

[1] M. Leblanc, V. Maisonneuve, A. Tressaud, Crystal Chemistry and Selected Physical Properties of Inorganic Fluorides and Oxide-Fluorides, Chem Rev 115(2) (2015) 1191-1254.
[2] P.P. Fedorov, A.A. Luginina, S.V. Kuznetsov, V.V. Osiko, Nanofluorides, J Fluorine Chem 132(12) (2011) 1012-1039.
[3] B.P. Sobolev, P.P. Fedorov, Phase diagrams of thE CaF2- (Y, Ln) F3 svstems I. Experimental, Journal of the Less Common Metals 60(1) (1978) 33-46.
[4] P.P. Fedorov, Systems of Alkali and Rare-Earth Metal Fluorides, Russian Journal of Inorganic Chemistry 44(11) (1999) 1703-1727.
[5] M. Boca, A. Rakhmatullin, J. Mlynarikova, E. Hadzimova, Z. Vaskova, M. Micusik, Differences in XPS and solid state NMR spectral data and thermo-chemical properties of iso-structural compounds in the series KTaF6, K2TaF7 and K3TaF8 and KNbF6, K2NbF7 and K3NbF8, Dalton T 44(39) (2015) 17106-17117.
[6] J.P. Chaminade, M. Vlasse, M. Pouchard, Hagenmul.P, SOME POTASSIUM OXYFLUOROTANTALATES, Bulletin De La Societe Chimique De France Partie I-Physicochimie Des Systemes Liquides Electrochimie Catalyse Genie Chimique (9-10) (1974) 1791-1794.
[7] M. Vlasse, A. Boukhari, J.P. Chaminade, M. Pouchard, Crystal structure of the potassium tantalum oxyfluoride K6Ta6.5O14.5F9.5, Materials Research Bulletin 14(1) (1979) 101-108.
[8] A. Rakhmatullin, M. Boča, J. Mlynáriková, E. Hadzimová, Z. Vasková, I.B. Polovov, M. Mičušík, Solid state NMR and XPS of ternary fluorido-zirconates of various coordination modes, J Fluorine Chem 208 (2018) 24-35.
[9] M. Boča, Z. Netriová, A. Rakhmatullin, Z. Vasková, E. Hadzimová, Ľ. Smrčok, O. Hanzel, B. Kubíková, The differing responses of various techniques in measuring the phase transformations of K2ZrF6, Journal of Molecular Liquids (2019) 110969.
[10] G.M. Sheldrick, Acta Cryst. A 64 (2008) 112-122.
[11] PLATON, A Multipurpose Crystallographic Tool, Utrecht University, Utrecht, The Netherlands, 2008.
[12] K. Brandenburg, M. Berndt, DIAMOND - Visual Crystal Structure Information System CRYSTAL IMPACT, Postfach 1251, D-53002 Bonn.
[13] Bruker AXS TOPAS V4: General profile and structure analysis software for powder diffraction data. – User's Manual, Bruker AXS, Karlsruhe, Germany, 2008.
[14] M. Boča, P. Barborík, M. Mičušík, M. Omastová, X-ray photoelectron spectroscopy as detection tool for coordinated or uncoordinated fluorine atoms demonstrated on fluoride systems NaF, K2TaF7, K3TaF8, K2ZrF6, Na7Zr6F31 and K3ZrF7, Solid State Sciences 14(7) (2012) 828-832.
[15] B. Kubíková, J. Mlynáriková, Z. Vasková, P. Jeřábková, M. Boča, Phase analysis and density of the system K2ZrF6–K2TaF7, Monatshefte für Chemie - Chemical Monthly 145(8) (2014) 1247-1252.
[16] L. Kosa, I. Mackova, I. Proks, O. Pritula, L. Smrcok, M. Boca, H. Rundlof, Phase transitions of K2TaF7 within 680-800 degrees C, Central European Journal of Chemistry 6(1) (2008) 27-32.
[17] B. Kubikova, M. Boca, M. Gaune-Escard, Phases of the K2TaF7-TaF5 binary system, Monatshefte Fur Chemie 139(6) (2008) 587-590.
[18] M. Boca, V. Danielik, Z. Ivanova, E. Miksikova, B. Kubikova, Phase diagrams of the KF-K2TaF7 and KF-Ta2O5 systems, Journal of Thermal Analysis and Calorimetry 90 (2007) 159-165.